Journal of Alloys and Compounds 619 (2015) 839–845

Contents lists available at ScienceDirect

Journal of Alloys and Compounds

journal homepage: www.elsevier.com/locate/jalcom

^{57}Fe Mössbauer spectroscopy and magnetic study of $Al_{13}Fe_4$

Mohammed A. Albedah [a], Farshad Nejadsattari [a], Zbigniew M. Stadnik [a,*], Janusz Przewoźnik [b]

[a] Department of Physics, University of Ottawa, Ottawa, Ontario K1N 6N5, Canada
[b] Solid State Physics Department, Faculty of Physics and Applied Computer Science, AGH University of Science and Technology, 30-059 Kraków, Poland

ARTICLE INFO

Article history:
Received 29 July 2014
Received in revised form 22 August 2014
Accepted 25 August 2014
Available online 10 September 2014

Keywords:
Paramagnet
^{57}Fe Mössbauer spectroscopy
Electric field gradient
Debye temperature

ABSTRACT

The results of *ab initio* electronic structure and electric field gradient (EFG) calculations, and of X-ray diffraction, ^{57}Fe Mössbauer spectroscopy, and magnetic studies of $Al_{13}Fe_4$ are reported. It is shown that $Al_{13}Fe_4$ crystallizes in the monoclinic space group $C2/m$, in which Fe atoms are located at five inequivalent crystallographic sites, with the lattice parameters $a = 15.503(2)$ Å, $b = 8.063(2)$ Å, $c = 12.464(2)$ Å, and $\beta = 107.71(2)^\circ$. We demonstrate that zero-field Mössbauer spectra can be decomposed into three quadrupole doublets. With the aid of the calculated EFG parameters we show that the first doublet results from one Fe site, the second doublet is due to two other Fe sites, and the third doublet originates from the last two Fe sites. We find that the shape of the Mössbauer spectrum of $Al_{13}Fe_4$ measured in an external magnetic field of 90 kOe can be accounted for with five component subspectra generated using the calculated EFG parameters at five inequivalent Fe sites. The quadrupole splittings corresponding to three component doublets are shown to increase with decreasing temperature and are well described by a $T^{3/2}$ power-law relation. The Debye temperature of $Al_{13}Fe_4$ is found to be 383(3) K. We find a pseudogap in the density of states (DOS), with a width of ~ 0.2 eV, that is centered 0.1 eV above the Fermi energy. The finite DOS at the Fermi energy confirms good metallicity of $Al_{13}Fe_4$. The $1/T$-like dependence of the magnetic susceptibility shows that $Al_{13}Fe_4$ is a paramagnet.

1. Introduction

Al-rich Fe aluminides form complex atomic structures. Examples of such structures are those of Al_2Fe [1], Al_5Fe_2 [2], and $Al_{13}Fe_4$ [3,4]. $Al_{13}Fe_4$ has been identified [5] as an approximant [6] to the decagonal quasicrystal [7]. The experimental studies of magnetic properties of these three compounds indicate that in none of them is a long-range magnetic order developed. The difficulty in studies of magnetic properties of these compounds lies in the fact that in both polycrystalline and single-crystal specimens a tiny fraction of a ferromagnetic second phase is unavoidably present. Al_2Fe (Refs. [8–10]) and Al_5Fe_2 (Refs. [11,10]) were shown to be spin glasses whereas $Al_{13}Fe_4$ was found to be a paramagnet [12,13].

Iron atoms are located at five inequivalent crystallographic sites in the monoclinic structure of $Al_{13}Fe_4$ [3,4]. Since the point symmetries of these sites are lower than cubic (Table 1), one could thus expect that the ^{57}Fe Mössbauer spectrum of $Al_{13}Fe_4$ should be a superposition of five quadrupole doublets [14]. In some Mössbauer studies [15–17] the spectra of $Al_{13}Fe_4$ were fitted with three single-Lorentzian-lineshape components, with no justification for the origin of these components. In other Mössbauer studies [12,18,19] the spectra at room temperature were fitted with two quadrupole-doublet components based on the following qualitative justification: Fe atoms in four 4*i* sites (Table 1) have similar asymmetric atomic environments and thus contribute to one quadrupole-doublet component, and Fe atoms in the 8*j* site have a less asymmetric atomic environment and thus contribute to another quadrupole-doublet component with a smaller quadrupole splitting [14]. As will be shown below from *ab initio* EFG calculations, this justification is incorrect.

The situation described above provides a strong motivation to revisit the ^{57}Fe Mössbauer spectra of $Al_{13}Fe_4$. With the aid of *ab initio* EFG calculations, we demonstrate that the shape of ^{57}Fe Mössbauer spectra of $Al_{13}Fe_4$ can be accounted for with three quadrupole-doublet components resulting from Fe atoms at five inequivalent crystallographic sites. We find that the quadrupole splittings corresponding to three component doublets increases with decreasing temperature and that their temperature dependence is well described by a $T^{3/2}$ power-law relation. We also determine the Debye temperature of $Al_{13}Fe_4$ and show that the studied compound is a paramagnet down to 2.0 K. We demonstrate the presence of a pseudogap around the Fermi energy in the electronic DOS of $Al_{13}Fe_4$.

* Corresponding author.
E-mail address: stadnik@uottawa.ca (Z.M. Stadnik).

http://dx.doi.org/10.1016/j.jallcom.2014.08.225
0925-8388/

Table 1
Crystallographic data [4] for $Al_{13}Fe_4$ and calculated V_{zz} (in units of 10^{21} V/m^2) and η.

Atom	Site	Point symmetry	x	y	z	V_{zz}	η
Fe(1)	4*i*	*m*	0.0851	0.0	0.3821	2.189	0.103
Fe(2)	4*i*	*m*	0.4018	0.0	0.6234	−2.308	0.532
Fe(3)	4*i*	*m*	0.0906	0.0	0.9889	−0.272	0.989
Fe(4)	4*i*	*m*	0.4031	0.0	0.9859	0.413	0.007
Fe(5)	8*j*	1	0.3195	0.2938	0.2777	2.337	0.399
Al(1)	4*i*	*m*	0.0649	0.0	0.1743	3.613	0.999
Al(2)	4*i*	*m*	0.3232	0.0	0.2819	−6.783	0.131
Al(3)	4*i*	*m*	0.2377	0.0	0.5349	−4.332	0.448
Al(4)	4*i*	*m*	0.0736	0.0	0.5803	1.723	0.832
Al(5)	4*i*	*m*	0.2406	0.0	0.9608	−4.972	0.377
Al(6)	4*i*	*m*	0.4792	0.0	0.8288	−3.707	0.924
Al(7)	2*d*	2/*m*	$\frac{1}{2}$	0.0	$\frac{1}{2}$	−4.742	0.868
Al(8)	4*i*	*m*	0.3057	0.0	0.7728	−1.495	0.059
Al(9)	4*i*	*m*	0.0870	0.0	0.7885	−2.498	0.160
Al(10)	8*j*	1	0.1850	0.2168	0.1106	−3.086	0.368
Al(11)	8*j*	1	0.3677	0.2113	0.1097	−3.389	0.152
Al(12)	8*j*	1	0.8217	0.7790	0.6654	−3.163	0.802
Al(13)	8*j*	1	0.4916	0.2334	0.3296	3.472	0.692
Al(14)	8*j*	1	0.3634	0.2188	0.4786	−3.584	0.444
Al(15)	4*g*	2	0.0	0.2496	0.0	4.690	0.739

2. Experimental methods

An ingot of nominal composition $Al_{13}Fe_4$ was prepared by inductive melting constituent elements in a water-cooled copper crucible under an argon atmosphere [20]. It was then annealed at 1223 K for 400 h and at 853 K for 24 h, followed by a slow cooling to room temperature.

X-ray diffraction measurements were carried out at 298 K in Bragg–Brentano geometry on a PANalytical X'Pert scanning diffractometer using Cu Kα radiation in the 2θ range 5–132° in steps of 0.02°. The $K\beta$ line was eliminated by using a Kevex PSi2 Peltier-cooled solid-state Si detector.

The dc magnetization was measured in the temperature range from 2.0 to 350 K and in magnetic fields up to 90 kOe using the vibrating sample magnetometer (VSM) option of the Quantum Design physical property measurement system (PPMS). The dc magnetic susceptibility was measured using PPMS in a magnetic field of 10 kOe in the temperature range of 2–390 K.

The ^{57}Fe Mössbauer measurements were conducted using standard Mössbauer spectrometers operating in sine mode and a 50-mCi ^{57}Co(Rh) source, which was kept at room temperature for zero-field measurements and at the same temperature as that of the absorber for an in-field measurement. The spectrometers used for zero-field and in-field measurements were calibrated, respectively, with a 6.35-μm-thick α-Fe foil [21] and a Michelson interferometer [22], and the spectra were folded. The Mössbauer absorber consisted of a mixture of powdered $Al_{13}Fe_4$, and powdered boron nitride, which was pressed into a pellet and put into a high-purity, 8-μm-thick Al disk container to ensure a uniform temperature over the whole absorber. The Mössbauer absorber was put into a Mössbauer cryostat in which it was kept in a static exchange gas atmosphere at a pressure of $\sim 7\times10^{-3}$ mbar. The surface density of the Mössbauer absorber was 9.8 mg/cm^2. This corresponds to an effective thickness parameter [14] $t_a = 2.2 f_a$, where f_a is the Debye-Waller factor of the absorber. Since $t_a > 1$, the resonance line shape of the Mössbauer spectra was described using a transmission integral formula [23]. The ^{57}Fe Mössbauer spectra were analyzed by means of a least-squares fitting procedure which entailed calculations of the positions and relative intensities of the absorption lines by numerical diagonalization of the full hyperfine interaction Hamiltonian [14].

Ab initio electronic structure and EFG calculations have been performed within the framework of density functional theory using the full-potential linearized augmented-plane-wave plus local orbitals (FP-LAPW+lo) method as implemented in the WIEN2k package [24].

3. Results and discussion

3.1. Structural characterization

The studied compound $Al_{13}Fe_4$ crystallizes in the monoclinic space group $C2/m$ (No. 12) [4]. There are 6 formula units of $Al_{13}Fe_4$ per unit cell, i.e., there are 102 atoms in a unit cell. Fig. 1 shows the crystal structure of $Al_{13}Fe_4$, and the atomic coordinates of the Al and Fe sites, taken from Ref. [4], are given in Table 1.

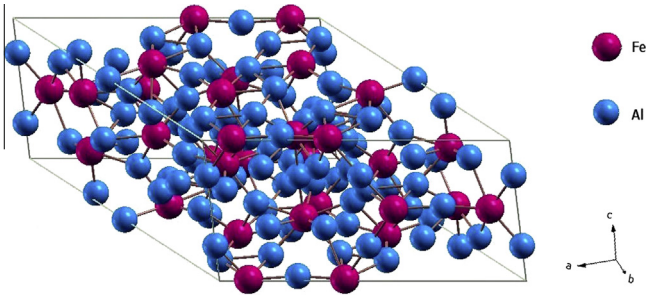

Fig. 1. The unit cell of the $Al_{13}Fe_4$ compound.

The X-ray powder diffraction pattern of $Al_{13}Fe_4$ is shown in Fig. 2. A Rietveld refinement [25] of the X-ray powder diffraction data was carried out using the atomic coordinates in Table 1, yielding the lattice parameters $a = 15.503(2)$ Å, $b = 8.063(2)$ Å, $c = 12.464(2)$ Å, and $\beta = 107.71(2)^\circ$. The values of these lattice parameters compare well with the corresponding values reported earlier [4]. No second phases could be detected in the X-ray powder diffraction pattern of $Al_{13}Fe_4$ (Fig. 2).

3.2. Electronic structure and EFG calculations

In the FP-LAPW+lo method used for the calculations, the unit cell is divided into non-overlapping muffin-tin (MT) spheres centered at nuclei, and an interstitial region. The wave functions in the interstitial regions are expanded in plane waves and the wave functions inside the MT spheres are linear combinations of radial functions times spherical harmonics. The exchange-correlation potential is calculated by the generalized gradient approximation, using the scheme developed by Perdew, Burke, and Ernzerhof [26]. The maximum orbital angular momentum for the expansion of the wave function in spherical harmonics inside the MT spheres was taken to be $l_{max} = 10$. The Brillouin zone integrations within the self-consistency cycles were performed via a tetrahedron method, using 115 k-points in the irreducible wedge of the Brillouin zone. To obtain as precise results as possible, we expanded the basis function up to $R_{MT} \times K_{MAX} = 7$, where R_{MT} is the smallest spherical muffin-tin radius present in the system and K_{MAX} is the maximum modulus of the reciprocal lattice vector. We adopted the values of 2.00 and 2.33 Å for Al and Fe, respectively, as the R_{MT} radii. In the calculations self-consistency was achieved by demanding the convergence of the integrated charge and energy difference between succeeding iterations to be smaller than 10^{-3} e and 10^{-3} Ry,

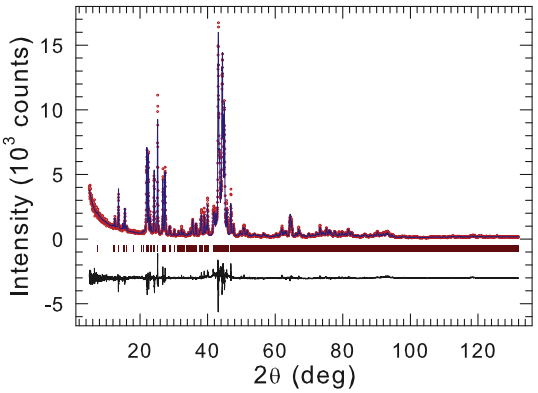

Fig. 2. Powder X-ray diffraction pattern of $Al_{13}Fe_4$ at 298 K. The experimental data are denoted by open circles, while the line through the circles represents the results of the Rietveld refinement. The row of vertical bars shows the Bragg peak positions for the $C2/m$ space group. The lower solid line represents the difference curve between experimental and calculated patterns.

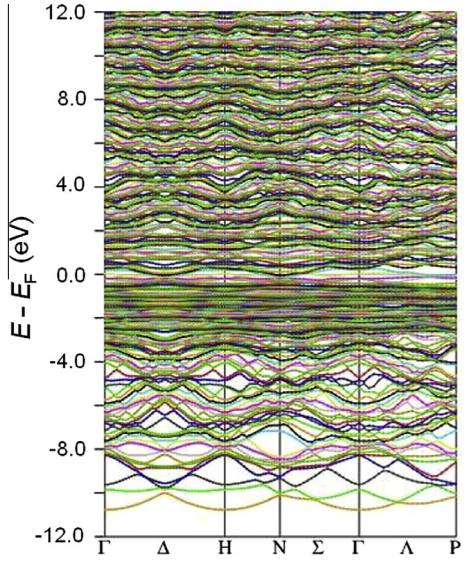

Fig. 3. Energy band structure of $Al_{13}Fe_4$.

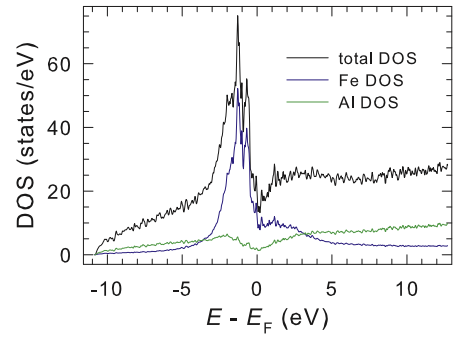

Fig. 4. Total electronic density of states (DOS) of $Al_{13}Fe_4$, and Fe and Al DOS.

respectively. The experimental lattice parameters (a, b, c, and β) and atomic coordinates (Table 1) were used.

The calculated electronic band structure of $Al_{13}Fe_4$ is shown in Fig. 3. It shows that the nature of the compound studied is metallic as the valence and conduction bands overlap around the Fermi energy. To the best of our knowledge, there are no experimental data on the band structure of this compound to be compared with our results.

Fig. 4 shows the total electronic DOS of $Al_{13}Fe_4$. The presence of a narrow pseudogap, with a width of ~ 0.2 eV, located at 0.1 eV above the Fermi energy E_F, is clearly visible. The existence of such a pseudogap in the DOS at or around E_F is a characteristic feature of the DOS of quasicrystals and their crystalline approximants. This pseudogap results either from Fermi surface – Brillouin zone interactions or from the strong hybridization of Fe d states with the Al s and p states [27,28]. Fig. 4 implies good metallicity of $Al_{13}Fe_4$ due to a finite DOS at E_F.

We calculated V_{zz} and the asymmetry parameter $\eta = (V_{xx} - V_{yy})/V_{zz}$ $(0 \leqslant \eta \leqslant 1)$, where V_{yy}, V_{xx}, and V_{zz} are the eigenvalues of the EFG tensor in order of increasing magnitude [14], at all Fe and Al crystallographic sites. The calculated V_{zz} and η values are displayed in Table 1 and their comparison with experiment will be discussed below.

3.3. Mössbauer spectroscopy

The room- and liquid-nitrogen temperature ^{57}Fe Mössbauer spectra of $Al_{13}Fe_4$ measured in a large velocity range are shown

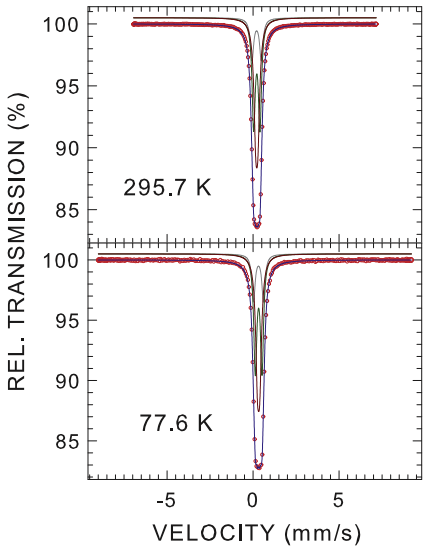

Fig. 5. Room- and liquid-nitrogen ^{57}Fe Mössbauer spectra of $Al_{13}Fe_4$ measured in a large velocity range fitted (blue solid line) with three quadrupole doublets (dark grey, dark green, and dark red solid lines), as described in the text. (For interpretation of the references to colour in this figure legend, the reader is referred to the web version of this article.)

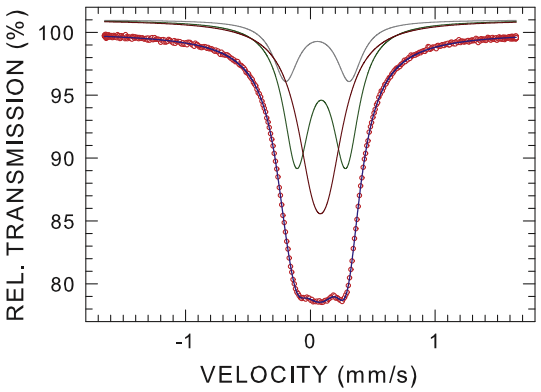

Fig. 6. ^{57}Fe Mössbauer spectrum of $Al_{13}Fe_4$ at 5.7 K fitted (blue solid line) with three quadrupole doublets (dark grey, dark green, and dark red solid lines), as described in the text. The zero-velocity origin is relative to the source at 5.7 K. (For interpretation of the references to colour in this figure legend, the reader is referred to the web version of this article.)

in Fig. 5. The spectra can be fitted well with three component quadrupole doublets (*vide infra*) and no Zeeman pattern originating from a possible magnetic impurity phase present in the studied specimen can be discerned in them.

A quadrupole splitting, i.e., the distance between two resonance lines in a ^{57}Fe Mössbauer quadrupole doublet, is given by [14]

$$\Delta = \frac{1}{2} eQ|V_{zz}|\sqrt{1+\eta^2/3}, \tag{1}$$

where e is the proton charge and Q is the electric quadrupole moment of the ^{57}Fe nucleus (0.15 b) [29].

A visual inspection of the Mössbauer spectrum of $Al_{13}Fe_4$ (Fig. 6) shows that it exhibits a three-valley structure. As there are five inequivalent Fe sites in the crystal structure of $Al_{13}Fe_4$ (Table 1), one could attempt to fit this spectrum with five quadrupole doublets. This, however, is impossible in practice as the structure of the spectrum is not rich enough to allow for a fit with the number of free parameters corresponding to five component quadrupole doublets. This spectrum can be very well fitted with the maximum,

practically possible, three component quadrupole doublets (Fig. 5(a)). The spectral weights of these three component doublets, in the order of decreasing Δ ($\Delta_a, \Delta_b, \Delta_c$,), are 15.7(1)%, 40.9(1)%, and 43.4(1)%. In what way are these three component doublets related to the five Fe sites, if they are related in any way at all?

A convincing indication of such a relation comes from the calculations of the EFG tensor at the five Fe sites. Using the calculated values of V_{zz} and η (Table 1), one would expect the Mössbauer spectrum of $Al_{13}Fe_4$ to be a superposition of five component quadrupole doublets with $\Delta_1 = 0.342, \Delta_2 = 0.377, \Delta_3 = 0.049, \Delta_4 = 0.064$, and $\Delta_5 = 0.374$ mm/s. One can see that $\Delta_3 \approx \Delta_4 \ll \Delta_1 \leqslant \Delta_2 \approx \Delta_5$. Thus, the component doublets Δ_a, Δ_b, and Δ_c can be associated with the Fe atoms at sites (Table 1) Fe(1), Fe(2) and Fe(5), and Fe(3) and Fe(4), respectively.

Fig. 7(a) shows a simulated Mössbauer spectrum resulting from a superposition of five quadrupole-doublet components with Δ_i values (i = 1,2,3,4,5) calculated above and with the same value of δ. One can observe that the simulated spectrum has a three-valley structure, although the experimental Δ_i values are larger than the calculated ones. However, this does not mean that the calculated Δ_i are imprecise; their precision is dictated by the accuracy of the Q value which is 13.3% [29]. The simulated spectrum generated with the Δ_i values larger by 14.0% than the theoretical ones (Fig. 7(b)) almost fits the experimental spectrum well.

Zero-field ^{57}Fe Mössbauer spectra of nonmagnetic polycrystalline compounds provide information only on the absolute value of the EFG (Eq. (1)). The sign of the EFG can be determined from ^{57}Fe Mössbauer spectra measured in external magnetic fields [30]. Fig. 8 shows a comparison between the ^{57}Fe Mössbauer spectrum of $Al_{13}Fe_4$ at 5.7 K measured in an external magnetic field of 90.0 kOe and the spectrum generated for the V_{zz} and η values in Table 1. Similarly to what has been done for calculating the simulated spectrum in Fig. 7(b), the values of V_{zz} were increased by 13.3%. If texture effects are negligible, one can assume that the principal axes of the EFG tensor are randomly oriented with respect to the external magnetic field. The algorithm for calculating the spectrum in such a case was given in Ref. [31] and was used here. We also assumed the same δ value for each of five component

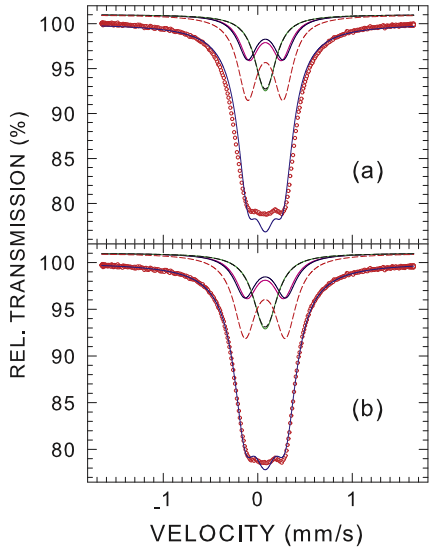

Fig. 7. (a) ^{57}Fe Mössbauer spectrum of $Al_{13}Fe_4$ at 5.7 K and simulated spectrum (blue solid line) resulting from the superposition of quadrupole doublets (with Δ values calculated from the data in Table 1) due to the Fe atoms at the Fe(1) site (pink solid line), Fe(2) site (dark blue solid line), Fe(3) site (green solid line), Fe(4) site (black short-dash line), and Fe(5) site (red short-dash line) (b) The same as in (a) but with Δ values increased by 14.0%. (For interpretation of the references to colour in this figure legend, the reader is referred to the web version of this article.)

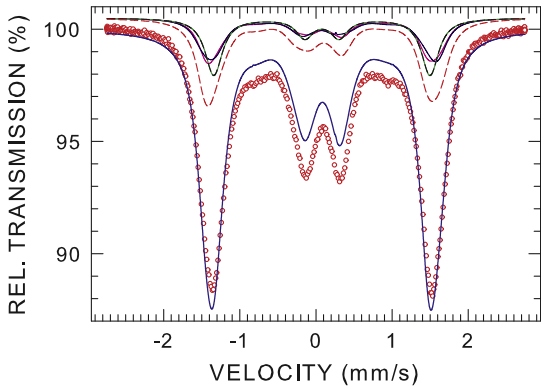

Fig. 8. Comparison of the ^{57}Fe Mössbauer spectrum of $Al_{13}Fe_4$ at 5.7 K measured in an external magnetic field of 90.0 kOe parallel to the direction of the γ rays (red open circles) with the simulated spectrum (blue solid line) resulting from the superposition of five component spectra, that were generated for the values of V_{zz} (multiplied by 1.14) and η in Table 1, due to the Fe atoms at the Fe(1) site (pink solid line), Fe(2) site (dark blue solid line), Fe(3) site (green solid line), Fe(4) site (black short-dash line), and Fe(5) site (red short-dash line). The zero-velocity origin is relative to the source at 5.7 K. (For interpretation of the references to colour in this figure legend, the reader is referred to the web version of this article.)

spectra. The structure of the in-field Mössbauer spectrum is relatively well accounted for by the simulated spectrum (Fig. 8). This provides additional support for the correctness of the calculated values of V_{zz} (magnitude and sign) and η at five Fe sites.

We note here in passing that a qualitative reasoning, used in previous Mössbauer studies of $Al_{13}Fe_4$ [12,18,19], affirming that, since the Fe atoms in four 4i sites have similar asymmetric atomic environments, they must therefore contribute to one quadrupole-doublet component, is unjustified. As one can see in Table 1, the values of V_{zz} at these four Fe sites are widely different.

Fig. 9 shows the ^{57}Fe Mössbauer spectra of $Al_{13}Fe_4$ measured in the temperature range 4.4–295.4 K. Excellent fits of these spectra are obtained with the three-quadrupole-doublet model discussed above. The values of Δ_i ($i = a, b, c$) derived from the fits of these spectra and of the spectrum in Fig. 6 are shown in Fig. 10(a)–(c). A clear increase of Δ_i with decreasing temperature is observed. Such a temperature dependence of Δ has been observed in many crystalline [32], quasicrystalline [33], and amorphous [34] compounds. It is well described by the empirical equation

$$\Delta(T) = \Delta(0)\left(1 - BT^{3/2}\right), \tag{2}$$

where $\Delta(0)$ is the value of Δ at 0 K and B is a constant. The fit of the $\Delta_i(T)$ data (Fig. 10(a)–(c)) to Eq. (1) gives $\Delta_a(0) = 0.564(3)$ mm/s, $B_a = 1.23(13) \times 10^{-5}$ K$^{-3/2}$, $\Delta_b(0) = 0.386(1)$ mm/s, $B_b = 1.20(7) \times 10^{-5}$ K$^{-3/2}$, and $\Delta_c(0) = 0.129(6)$ mm/s, $B_c = 1.11(15) \times 10^{-5}$ K$^{-3/2}$. The values of B_i are similar to those found for other compounds [32–34].

The absorption spectral area A of a Mössbauer spectrum is proportional to f_a, which is given in the Debye theory by [14]

$$f_a(T) = \exp\left\{-\frac{3}{4}\frac{E_\gamma^2}{Mc^2 k_B \Theta_D}\left[1 + 4\left(\frac{T}{\Theta_D}\right)^2 \int_0^{\Theta_D/T} \frac{x\,dx}{e^x - 1}\right]\right\}, \tag{3}$$

where M is the mass of the Mössbauer nucleus, c is the speed of light, E_γ is the energy of the Mössbauer transition, and Θ_D is the Debye temperature. Fig. 10(d) shows the temperature dependence of the spectral area A derived from the fits of the Mössbauer spectra in Fig. 9. The fit of the $A(T)$ data (Fig. 10(d)) to Eq. (3) yields $\Theta_D = 383(3)$ K. The value of Θ_D found here is close to the value of 419(5) K found in another Mössbauer study of $Al_{13}Fe_4$ [17,19], but is significantly smaller than the value of 544 K derived from specific-heat measurements [13].

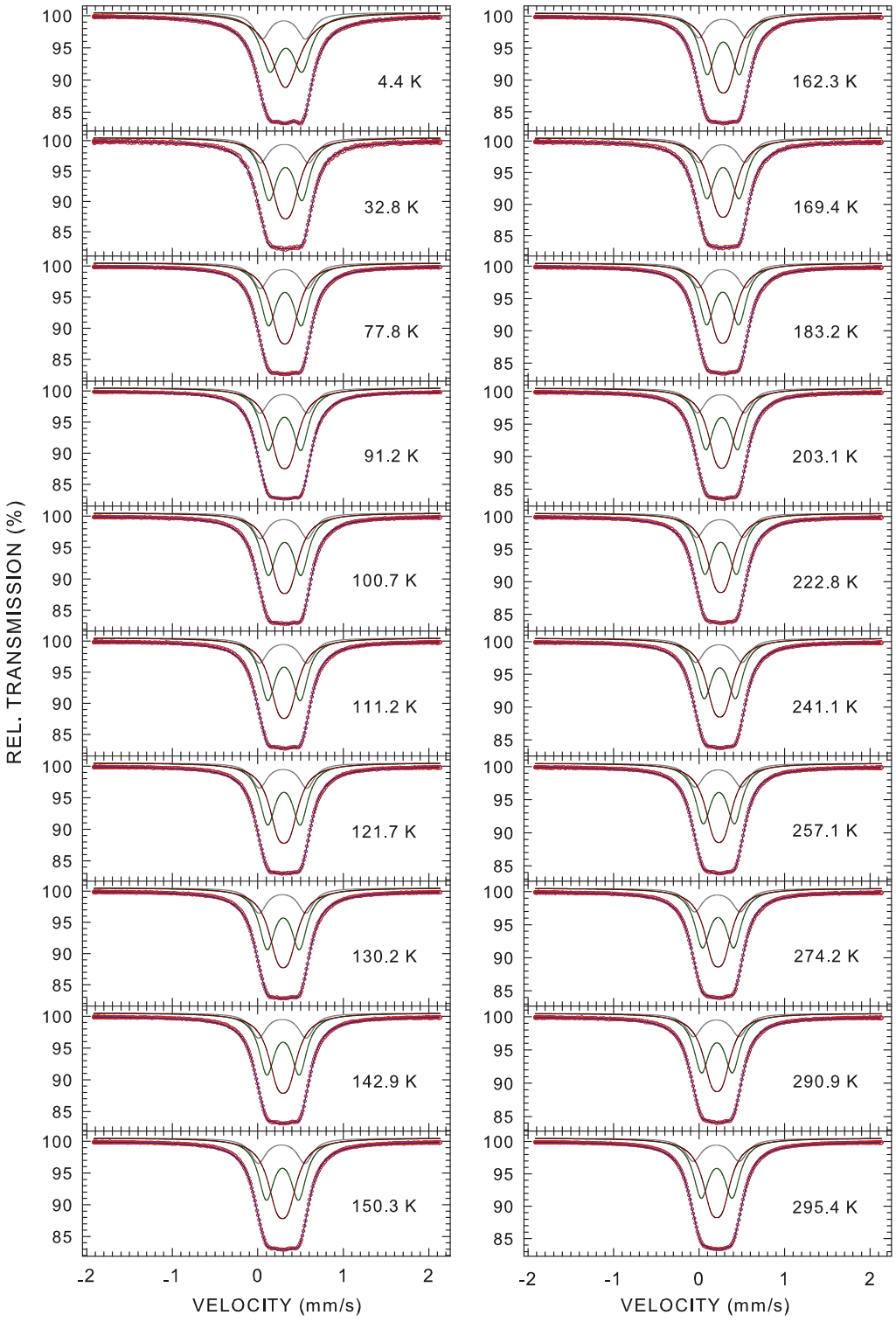

Fig. 9. ^{57}Fe Mössbauer spectra of $Al_{13}Fe_4$ at the indicated temperatures fitted (blue solid line) with three quadrupole doublets (dark grey, dark green, and dark red solid lines), as described in the text. The zero-velocity origin is relative to α-Fe at room temperature. (For interpretation of the references to colour in this figure legend, the reader is referred to the web version of this article.)

3.4. Magnetic measurements

Although the Mössbauer spectra in Fig. 3 show no presence of a possible magnetic impurity in the specimen studied (at the level of ~1 wt%), the magnetic field dependence of magnetization curves $M(H)$ measured at selected temperatures (Fig. 11) are typical for a ferromagnet. They show that M does not saturate in the highest field available of 90 kOe. Clearly, the studied specimen does contain a ferromagnetic impurity (at the ppm concentration level), probably in the form of an iron-oxide phase at the sample's surfaces or precipitated iron superparamagnetic clusters.

The temperature dependence of the magnetic susceptibility χ of $Al_{13}Fe_4$ measured in an applied magnetic field of 10 kOe is shown in Fig. 12. It follows approximately a $1/T$-like dependence

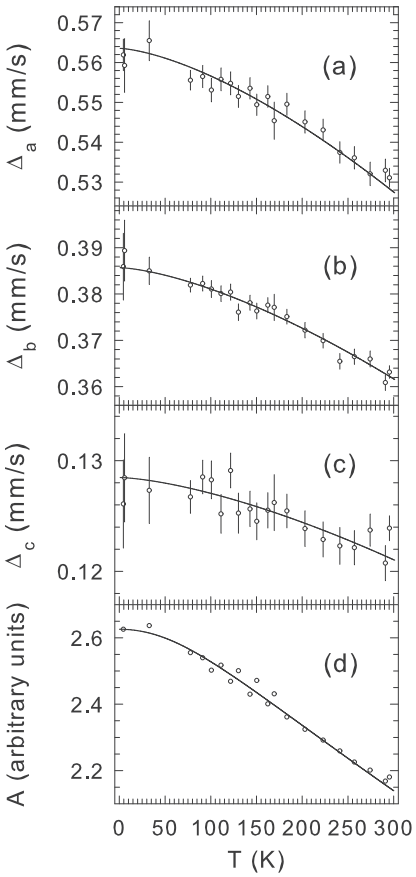

Fig. 10. Temperature dependence of (a) the quadrupole splittings Δ_i ($i = a, b, c$) and (b) the absorption spectral area A of $Al_{13}Fe_4$. The solid lines are the fits to Eq. (2) in (a) and to Eq. (3) in (b), as explained in the text.

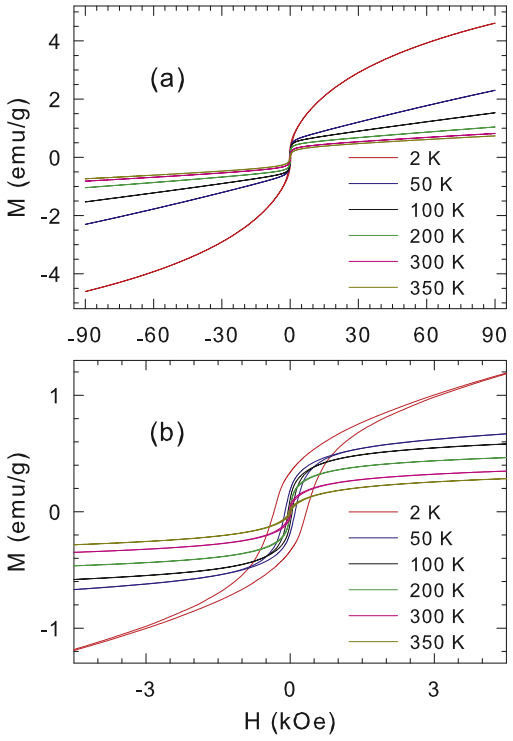

Fig. 11. $M(H)$ curves of $Al_{13}Fe_4$ at selected temperatures in the magnetic field range −90 – +90 kOe (a) and −4.5 – +4.5 kOe (b)

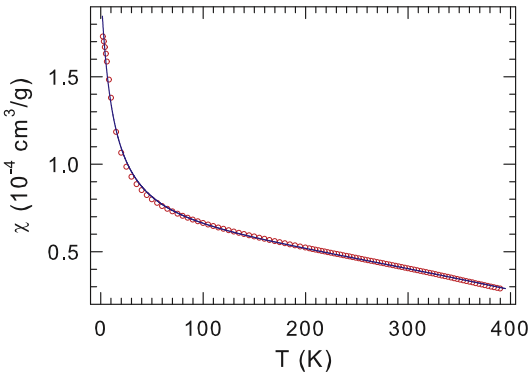

Fig. 12. Temperature dependence of the magnetic susceptibility of $Al_{13}Fe_4$ measured in an external magnetic field of 10 kOe. The solid line is the fit to Eq. (4), as explained in the text.

characteristic of the Curie–Weiss law. To allow for the presence in the studied specimen of a small amount of ferromagnetic impurity with the saturation magnetization M_0, the $\chi(T)$ data were fitted to the equation containing an additional $T^{3/2}$ term associated with Bloch spin-waves [12,35]

$$\chi = \chi_0 + \frac{C}{T - \Theta_p} + \frac{M_0}{H}\left(1 - a_{3/2}T^{3/2}\right), \tag{4}$$

where χ_0 is the temperature-independent term that includes contributions from Pauli and Van Vleck paramagnetism as well as core and Landau diamagnetism, C is the Curie constant, and Θ_p is the paramagnetic Curie temperature. The Curie constant can be expressed as $C = \frac{N\mu_{eff}^2}{3k_B}$, where N is the number of Fe atoms per formula unit, μ_{eff} is the effective magnetic moment, and k_B is the Boltzmann constant. The value of $M_0 = 2.53$ emu/g used in the fit was estimated from a linear extrapolation of the 2 K $M(H)$ curve (Fig. 11(a)) to $H = 0$. The fit of the $\chi(T)$ data (Fig. 12)) to Eq. (4) gives $\chi_0 = 2.62(3) \times 10^{-5}$ cm^3/g, $C = 1.77(6) \times 10^{-3}$ cm^3 K/g, and $\Theta_p = -12.0(5)$ K. The value of C corresponds to $\mu_{eff} = 1.42(1)\ \mu_B$ per Fe atom.

4. Summary

We report the results of *ab initio* electronic structure and EFG calculations, and of X-ray diffraction, magnetic and ^{57}Fe Mössbauer spectroscopy studies of $Al_{13}Fe_4$. The studied alloy is shown to crystallize in the monoclinic space group $C2/m$ with the lattice parameters $a = 15.503(2)$ Å, $b = 8.063(2)$ Å, $c = 12.464(2)$ Å, and $\beta = 107.71(2)^\circ$. Excellent fits of the zero-field Mössbauer spectra are obtained with three component quadrupole doublets which are shown to result from Fe atoms located at five inequivalent crystallographic sites. We find that the quadrupole splittings corresponding to three component doublets increase with decreasing temperature and are well described by a $T^{3/2}$ power-law relation. The shape of the Mössbauer spectrum of $Al_{13}Fe_4$ measured in an external magnetic field of 90 kOe is well accounted for with five component subspectra generated using the calculated EFG parameters at five inequivalent Fe sites. We find that the Debye temperature of $Al_{13}Fe_4$ is 383(3) K. The DOS calculations predict the presence of a pseudogap located at 0.1 eV above E_F and with a width of ~ 0.2 eV. Good metallicity of $Al_{13}Fe_4$ is confirmed by the calculated finite DOS at E_F. The studied compound is shown to be a paramagnet down to 2.0 K.

Acknowledgements

This work was supported by the Natural Sciences and Engineering Research Council of Canada. The computational work was conducted using the High Performance Computing Virtual Laboratory (www.hpcvl.org) computing facility. We thank N. Benabou (HPCVL) for technical help with WIEN2k and B. Grushko for providing the sample of $Al_{13}Fe_4$.

References

[1] R.N. Corby, P.J. Black, Acta Crystallogr. Sec. B 29 (1973) 2669.
[2] U. Burkhardt, Yu. Grin, M. Ellner, K. Peters, Acta Crystallogr. Sec. B 50 (1994) 313.
[3] P.J. Black, Acta Crystallogr. 8 (1955) 43;
P.J. Black, Acta Crystallogr. 8 (1955) 175.
[4] J. Grin, U. Burkhardt, M. Ellner, K. Oeters, Z. Kristallogr. 209 (1994) 479.
[5] T. Fujiwara, T. Yokokawa, Phys. Rev. Lett. 66 (1991) 333.
[6] Z.M. Stadnik, in: K.H.J. Buschow (Ed.) Handbook of Magnetic Materials, (Elsevier, Amsterdam, 2013), Vol. 21, p. 77.
[7] C. Janot, Quasicrystals, A Primer, 2nd ed., Oxford University Press, Oxford, 1994.
[8] C.S. Lue, Y. Öner, D.G. Naugle, J.H. Ross Jr., Phys. Rev. B 63 (2001) 184405.
[9] J. Chi, Y. Li, F.G. Vagizov, V. Goruganti, J.H. Ross Jr., Phys. Rev. B 71 (2005) 024431.
[10] Z. Jagličić, S. Vrtnik, M. Feuerbacher, J. Dolinšek, Phys. Rev. B 83 (2011) 224427.
[11] J. Chi, X. Zheng, S.Y. Rodriguez, Y. Li, W. Gou, V. Goruganti, K.D.D. Rathnayaka, J.H. Ross Jr., Phys. Rev. B 82 (2010) 174419.
[12] F. Müller, M. Rosenberg, W. Liu, U. Köster, Mater. Sci. Eng. A 134 (1991) 900.
[13] P. Popčević, A. Smontara, J. Ivkov, M. Wencka, M. Komelj, P. Jeglič, S. Vrtnik, M. Bobnar, Z. Jagličić, B. Bauer, P. Gille, H. Borrmann, U. Burkhardt, Yu. Grin, J. Dolinšek, Phys. Rev. B 81 (2010) 184203.
[14] N.N. Greenwood, T.C. Gibb, Mössbauer Spectroscopy, Chapman and Hall, London, 1971;
P. Gütlich, E. Bill, A. Trautwein, Mössbauer Spectroscopy and Transition Metal Chemistry, Springer, Berlin, 2011.
[15] R.S. Preston, R. Gerlach, Phys. Rev. B 3 (1971) 1519.
[16] C.A. Stickels, R.H. Bush, Met. Trans. 2 (1971) 2031.
[17] S.D. Forder, J.S. Brooks, P.V. Evans, Scripta Mater. 35 (1996) 1167.
[18] C.M. Chittaranjan, V. Kumar, B. Viswanathan, K.P. Gopinathan, Solid State Commun. 79 (1991) 69.
[19] S.D. Forder, J.S. Brooks, A. Reeder, P.V. Evans, Hyperfine Interact. 116 (1998) 209.
[20] R. Würschum, T. Troev, B. Grushko, Phys. Rev. B 52 (1995) 6411.
[21] Certificate of Calibration, Iron Foil Mössbauer Standard, Natl. Bur. Stand. (U.S.) Circ. No. 1541, edited by J.P. Cali (U.S. GPO, Washington, D.C., 1971).
[22] B.F. Otterloo, Z.M. Stadnik, A.E.M. Swolfs, Rev. Sci. Instrum. 54 (1983) 1575.
[23] S. Margulies, J.R. Ehrman, Nucl. Instrum. Methods 12 (1961) 131;
G.K. Shenoy, J.M. Friedt, H. Maletta, S.L. Ruby, in: I.J. Gruverman, C.W. Seidel, D.K. Dieterly (Eds.), Mössbauer Effect Methodology, Vol. 10, Plenum, New York, 1974, p. 277.
[24] P. Blaha, K. Schwartz, G. Madsen, D. Kvasnicka, J. Luitz, WIEN2k, An Augmented Plane Wave Plus Local Orbitals Program for Calculating Crystal Properties, Karlheinz Schwarz, Technical Universität Wien, Austria, 1999.
[25] R.A. Young, The Rietveld Method, Oxford University Press, Oxford, 1993.
[26] J.P. Perdew, S. Burke, M. Ernzerhof, Phys. Rev. Lett. 77 (1996) 3865.
[27] T. Fujiwara, in: Z.M. Stadnik (Ed.), Physical Properties of Quasicrystals, Springer-Verlag, Berlin, 1999, p. 169;
Y. Ishii, T. Fujiwara, in: T. Fujiwara, Y. Ishii (Eds.), Quasicrystals, Elsevier, Amsterdam, 2008, p. 171.
[28] U. Mizutani, M. Inukai, H. Sato, E.S. Zijlstra, Chem. Soc. Rev. 41 (2012) 6799.
[29] G. Martínez-Pinedo, P. Schwerdtfeger, E. Caurier, K. Langanke, W. Nazarewich, T. Söhnel, Phys. Rev. Lett. 87 (2001) 062701.
[30] Z.M. Stadnik, G. Zhang, Hyperfine Interact. 169 (2006) 1291;
Z.M. Stadnik, Solid State Commun. 51 (1984) 79.
[31] N. Blaes, H. Fisher, U. Gonser, Nucl. Instrum. Methods Phys. Res. B 9 (1985) 201.
[32] M.A. Albedah, K. Al-Qadi, Z.M. Stadnik, J. Przewoźnik, J. Alloys Compd. 613 (2014) 344;
Z.M. Stadnik, P. Wang, J. Żukrowski, T. Noji, Y. Koike, J. Phys.: Condens. Matter 25 (2013) 416008;
P. Wang, Z.M. Stadnik, J. Żukrowski, A. Thaler, S.L. Bud'ko, P.C. Canfield, Phys. Rev. B 84 (2011) 024509.
[33] K. Al-Qadi, P. Wang, Z.M. Stadnik, J. Przewoźnik, Phys. Rev. B 79 (2009) 224202;
Z.M. Stadnik, G. Zhang, J. Phys.: Condens. Matter 17 (2005) 6599;
Z.M. Stadnik, T. Takeuchi, N. Tanaka, U. Mizutani, J. Phys.: Condens. Matter 15 (2003) 6365.
[34] Z.M. Stadnik, Ö. Rapp, V. Srinivas, J. Saida, A. Inoue, J. Phys.: Condens. Matter 14 (2002) 6883;
M. Mao, D.H. Ryan, Z. Altounian, Hyperfine Interact. 92 (1994) 2163;
P. Deppe, M. Rosenberg, Hyperfine Interact. 15-16 (1993) 735.
[35] Z.M. Stadnik, F. Müller, Philos. Mag. B 71 (1995) 221.